ARTICLE

doi:10.1038/nature12295

Locomotion dynamics of hunting in wild cheetahs

A. M. Wilson[1], J. C. Lowe[1], K. Roskilly[1], P. E. Hudson[1]†, K. A. Golabek[2]† & J. W. McNutt[2]

Although the cheetah is recognised as the fastest land animal, little is known about other aspects of its notable athleticism, particularly when hunting in the wild. Here we describe and use a new tracking collar of our own design, containing a combination of Global Positioning System (GPS) and inertial measurement units, to capture the locomotor dynamics and outcome of 367 predominantly hunting runs of five wild cheetahs in Botswana. A remarkable top speed of 25.9 m s^{-1} (58 m.p.h. or 93 km h^{-1}) was recorded, but most cheetah hunts involved only moderate speeds. We recorded some of the highest measured values for lateral and forward acceleration, deceleration and body-mass-specific power for any terrestrial mammal. To our knowledge, this is the first detailed locomotor information on the hunting dynamics of a large cursorial predator in its natural habitat.

Measurements of instantaneous speed, acceleration and manoeuvring during athletic competition or hunting are rare[1–4], even for humans, horses and dogs, the most studied species. The cheetah (*Acinonyx jubatus*) is acknowledged as the ultimate cursorial predator, and its published[5] top speed of 29 m s^{-1} is considerably faster than racing speeds for greyhounds[2] (18 m s^{-1}), horses[1] (19 m s^{-1}) or humans (12 m s^{-1}; see 'Analysis of Bolt's 100m' at http://berlin.iaaf.org/records/biomechanics/index.html). Quantitative measurements of cheetah locomotion mechanics have only been made on captive animals chasing a lure in a straight line, with few studies eliciting speeds faster than racing greyhounds[6,7]. For wild cheetahs, estimates of speed and track have been made from direct observation or film only, and are limited to open habitat[8,9] and daylight hours.

Tracking collar design

To collect free-ranging locomotion data on wild cheetahs during hunting in their normal environment, we designed and built a tracking collar similar in size and weight to a conventional wildlife collar[10,11] (Fig. 1a; mass of 340 g), equipped with a GPS module capable of delivering processed position and velocity data, and raw pseudo-range, phase and Doppler data for individual satellite signals at 5 Hz, and an inertial measurement unit (IMU) consisting of triaxial microelectromechanical systems (MEMS) accelerometers, gyroscopes and magnetometers (Methods). The collar was powered by a rechargeable battery charged from solar cells, plus a non-rechargeable auxiliary battery. Data download and configuration upload was via radio. Collar software monitored the accelerometers to create activity summaries and detect the brief hunting events, buffered accelerometer data to capture the start of hunts, and adapted collar operation to battery voltages, time of day and activity. We increased the effective sample rate of the positioning system to 300 Hz, and reduced noise in the kinematic parameters, by fusing data from GPS and the IMU with a loosely coupled extended Kalman smoother (Methods). This was especially important during hunting because GPS accuracy was degraded both during initialization, and under conditions of high acceleration and high jerk[12].

Collection of hunting data

We recorded GPS–IMU data from 367 runs by three female and two male adult cheetahs (100, 66, 61 and 84, 56 runs respectively) over 17 months. A further 530 runs were identified in the activity data because the collar did not trigger on every run owing to the time of day and conservative trigger thresholds. An episode of feeding after a run indicated hunting success, and was identified in the activity data

Figure 1 | Cheetah with collar and anatomical features contributing to performance. **a**, Cheetah with a mark 2 collar is shown. **b**, Gravitational and centripetal accelerations acting on a turning cheetah; g denotes acceleration due to gravity, $v^2 r^{-1}$ denotes centripetal acceleration, and a is the resultant acceleration (effective gravity). **c**, Non-retractable cheetah claws that enhance grip. **d**, Low posture used in deceleration, which prevents pitching and engages hind limb musculature to absorb kinetic energy.

[1]Structure & Motion Laboratory, The Royal Veterinary College, University of London, Hatfield AL9 7TA, UK. [2]Botswana Predator Conservation Trust, Private Bag 13, Maun, Botswana. †Present addresses: Department of Sport and Exercise Sciences, University of Chichester, College Lane, Chichester, West Sussex PO19 6PE, UK (P.E.H.); Botswana Predator Conservation Trust, Private Bag 13, Maun, Botswana, and Wildlife Conservation Research Unit, Department of Zoology, University of Oxford, Oxford OX13 5QL, UK (K.A.G.)

by consistent, low-magnitude acceleration on all three axes[13] and was confirmed on a subset of hunts with field observations (Methods). Run routes were overlaid on Google Earth to identify terrain. The total number of GPS fixes recorded depended on activity, with an average of 180 ± 171 (mean ± s.d.) per cheetah per day, and a range of 7 to 1,571.

Runs started with a period of acceleration, either from stationary or slow movement (presumably stalking) up to high speed (Fig. 2). The cheetahs then decelerated and manoeuvred before prey capture. About one-third of runs involved more than one period of sustained acceleration (all 369 runs are presented in Supplementary Video 2). In successful hunts, there was often a burst of accelerometer data after the speed returned to zero, interpreted as the cheetah subduing the prey.

As well as hunting runs, cheetahs play and run from larger predators, but we had insufficient data validated by direct observations to provide secure separation of these activities, although only a few runs did not involve the tight turns and rapid speed changes characteristic of hunting (for example, runs 5, 32 and 49 in Supplementary Video 2). We therefore compared successful hunts to all other runs recorded by the collar. In total, 94 of the 367 runs (26%) were successful hunts. Including the 530 additional runs detected solely from IMU data did not change the success rate (223 out of 897; 25% success), which is lower than previously reported for individual cheetah[9,14,15], perhaps due, in part, to the inclusion of non-hunting runs. Cheetah are reported to move in predominantly open habitats using vegetation-edge to stalk their prey, often at dawn and dusk[8,9,14–16]. Although almost half of the runs here occurred at/after dawn, runs occurred throughout the day and night (Fig. 3e). The individual cheetahs varied in their predilection for running in open grassland or dense shrub (Supplementary Fig. 6). On average, the cheetahs ran most often in open habitat (48%, 176 of 367 runs); 28% of runs occurred in open shrub/around large trees, and 24% occurred within dense vegetation. Only 20% of runs occurring in the open grasslands were identified as successful hunts, compared with 31% of runs in dense cover. This difference in outcome was not significant ($P = 0.054$, chi-squared test) and is confounded by individual variation and habitat, but it does demonstrate that cheetahs do hunt successfully in all terrains[8,15]. Vegetation may confer an advantage by permitting stalking and limiting prey options for escape by manoeuvring; however, there was little difference in the distance or speed between terrains (Supplementary Table 1).

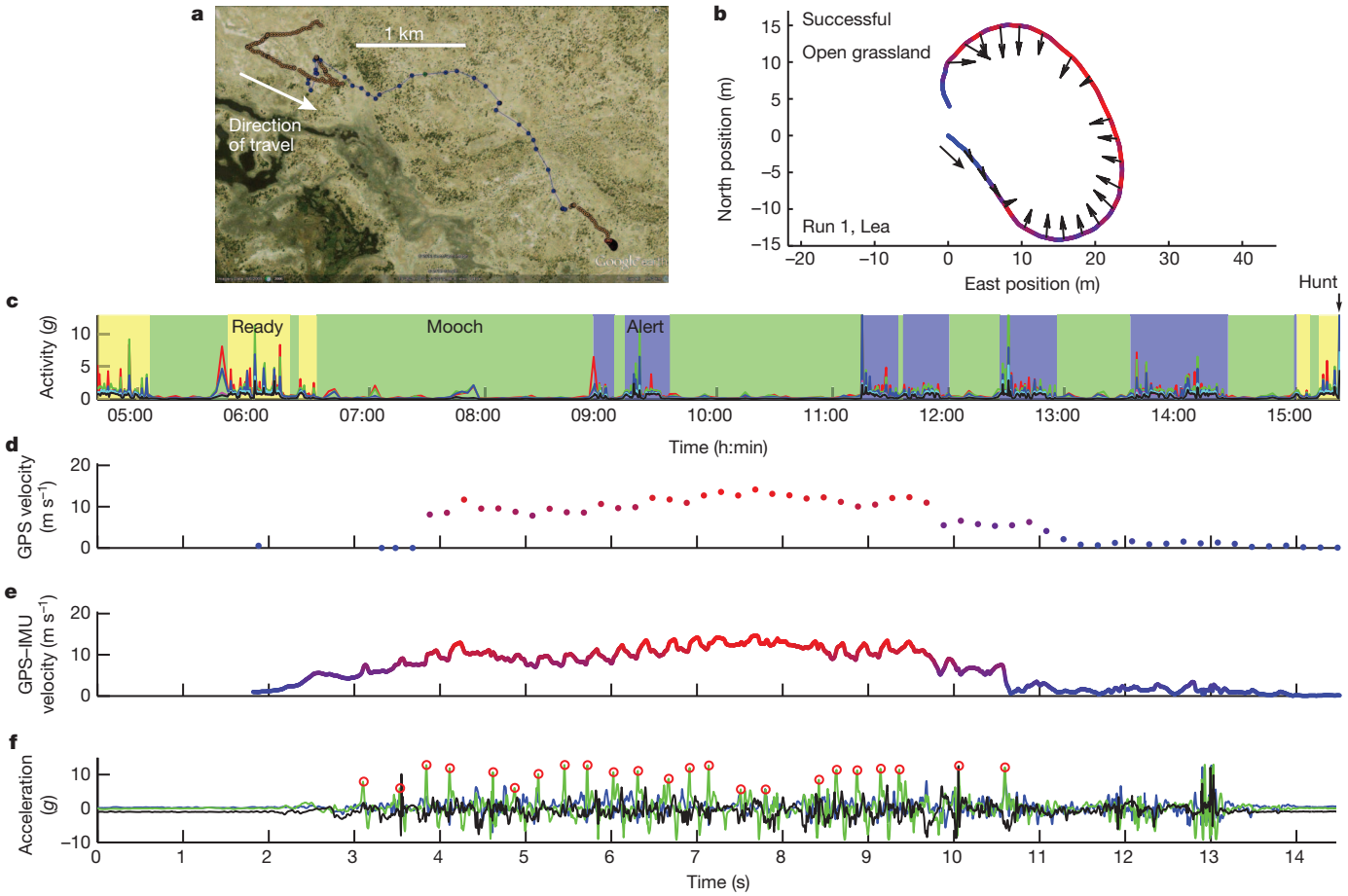

Figure 2 | An example day and hunt. **a**, Track of cheetah over 11 h (GPS data are available as a Google Earth file in Supplementary File 1). Each circular mark represents a GPS-derived position. Cheetah track and marks are colour-coded to collar state (detailed in Supplementary Fig. 1) as follows: alert, blue; mooch, green; ready, yellow; chase, red. **b**, Hunt track magnified from bottom right of **a**, hunt track is anticlockwise and marked with an arrow. Warmer (bright red) colours on track represent higher speed. **c**, Activity summary calculated in the collar from the accelerometer (Methods) for the 11-h period shown in **a**; shaded regions of the graph represent collar states as labelled. Line colours: peak accelerometer signal amplitude recorded in each 30-s period *X*, blue; *Y*, green; *Z*, red; mean of peak amplitude values extracted for each 2-s in each 30-s (that is, 15 bins) period *X*, cyan; *Y*, magenta; *Z*, black. The relative values for each axis differentiate between a single high-acceleration cycle and consistent movement in the 30-s window. Coordinate system: *X* lateral, positive left, *Y* fore–aft, positive forwards, *Z* vertical, positive upwards. Time is local (coordinated universal time (UTC) + 2 h). 'Hunt' time is labelled. **d**, Doppler-derived velocity profile for hunt determined by the GPS receiver at five updates per second. **e**, GPS–IMU-derived velocity profile for the chase; in **b**, **d** and **e** warmer (bright red) colours represent faster speeds. **f**, Accelerometer data recorded at 300 Hz for chase; *X*, blue; *Y*, green; *Z*, black. Red circles indicate forward acceleration peak used as event marker for stride cutting at, approximately, hindlimb foot contact. The high accelerations at zero velocity at $t = 12–13$ s suggest subduing prey and a successful hunt. An animation of a hunt is in Supplementary Video 1, plots of further runs are available in Supplementary Fig. 5, and all runs are in Supplementary Video 2.

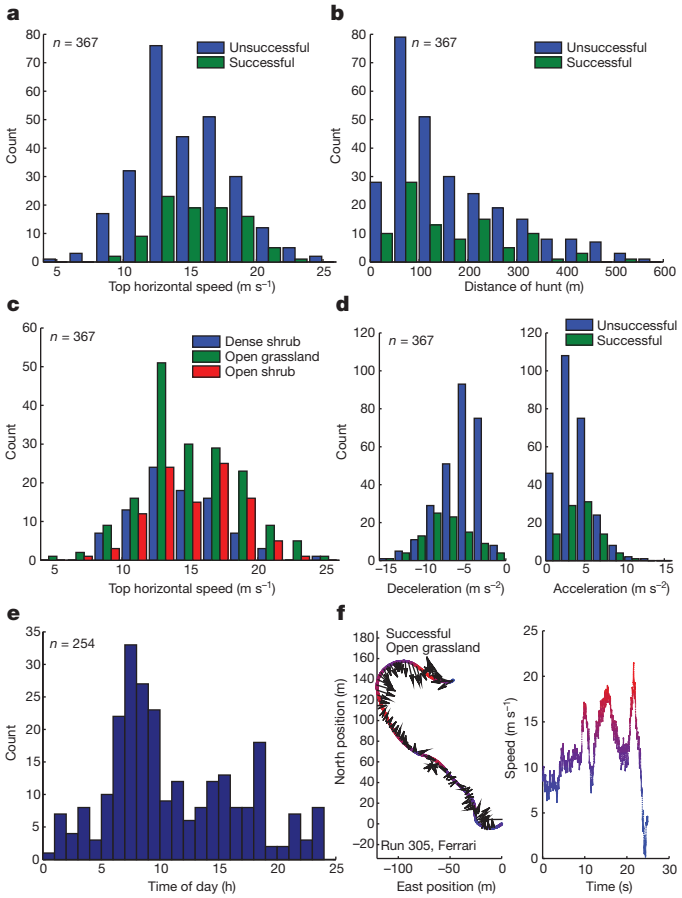

Figure 3 | Descriptive hunt statistics. **a**, Top speed, averaged over a stride, reached in each run colour-coded for outcome. **b**, Distance covered in each run. **c**, Top speed in each run coded for terrain type. **d**, Peak acceleration and deceleration recorded in each run. **e**, Plot of time of day of runs recorded in period when collar was set to trigger at any time of day, time local. **f**, Example hunt file colour-coded for speed (bright red denotes fastest), and with horizontal acceleration vectors drawn, to scale, for each stride. $n = 367$ (**a**–**d**) and $n = 254$ (**e**).

Description of hunts

The average run distance was 173 m (±116 m) (Fig. 3b) though recorded run distance will be shorter than the true value in the runs where the start of the run was missed (Methods, Supplementary Video 2). The longest runs recorded by each cheetah ranged from 407 to 559 m; the mean run frequency (including information from activity data) was 1.3 times per day, so, even if some hunts were missed, high speed locomotion only accounted for a small fraction of the 6,040-m average daily total distance covered by the cheetahs. The mean top speed was 14.9 ± 3.4 m s^{-1} and was usually only sustained for 1–2 s. The highest speed we recorded was a stride-averaged 25.9 m s^{-1} in run 250 (Fig. 3a, c and Supplementary Video 2). The top speeds attained by the other cheetahs were 25.4, 22.0, 21.1 and 20.1 m s^{-1}. The cheetahs studied here mostly hunted impala (*Aepyceros melampus*)[17], which made up 75% of their diet, although one male cheetah (Qamar), which frequently hunted in thicker vegetation (Supplementary Fig. 6), never exceeded 20.1 m s^{-1} and was often observed on warthog (*Phacochoerus africanus*) kills. Cheetah hunting the (anecdotally) faster Thompson's gazelle (*Eudorcas thomsonii*) on open East African savannah may use higher speeds.

Successful hunts involved greater deceleration on average (−7.5 m s^{-2} versus −5.5 m s^{-2}; $P < 0.05$; Fig. 3d), but there was no significant difference in peak acceleration (Fig. 3d), distance travelled (Fig. 3b) number of turns (6.7 versus 6.5) or total turn angle (347° versus 260°) (generalized linear mixed model (GLMM); Methods). This indicates that outcome was determined in the final stages of a hunt rather than hunts being abandoned early to save energy or reduce risk of injury, and the higher deceleration values may reflect actual prey capture. Equivalent locomotion and outcome data for coalition-hunting cheetah might clarify the importance of the final manoeuvring phase in hunt outcome.

Comparison with other athletic animals

The greatest acceleration and deceleration values were almost double values published for polo horses[18] and exceeded the accelerations reported for greyhounds at the start of a race[18]. The cheetahs sped up by up to 3 m s^{-1} and slowed by up to 4 m s^{-1} in a single stride (Supplementary Fig. 5d). Mass-specific change in kinetic energy over a stride (Fig. 4c and Supplementary Fig. 7) exceeded 30 J kg^{-1} stride^{-1} across the broad speed range of 10 to 18 m s^{-1}. On the basis of forward acceleration, the greatest stride-averaged whole animal powers often exceeded 100 W kg^{-1} (body mass) (Fig. 4d), and also occurred between 10 and 18 m s^{-1}. For comparison, we calculated a stride-averaged power of 25 W kg^{-1} for Usain Bolt's 9.58-s 100-m world record (Methods and http://berlin.iaaf.org/records/biomechanics/index.html), consistent with other measurements on human sprinters[19]; polo horses achieve 30 W kg^{-1} (ref. 18) and racing greyhounds 60 W kg^{-1} (ref. 18).

The locomotor (limb and back) muscle accounts for 45 ± 4% of body mass[20,21] in captive cheetah. The wild cheetahs had similar limb and back lengths to those captive cheetahs, but were heavier at 53 kg versus 33 kg (means, $n = 5, 5$), and visibly more muscled (mean mid-thigh girth 540 mm versus 450 mm, $n = 5, 5$), so much of their body mass is locomotor muscle. Major propulsive muscles such as the hamstrings (biceps femoris, semimembranosus and semitendinosus) at the hip and gastrocnemius at the tarsus have 64% and 60% longer moment arms, respectively, than in the greyhound and similar muscle fibre lengths[21]. Stride frequency and posture are similar at the same speed in the two species[7] so the muscle sarcomeres (and fibres) will be shortening considerably faster in the cheetah than in the greyhound at the same speed (like the engine of a car in a lower gear). This fast muscle contraction velocity will enable large muscle powers and hence deliver the very large acceleration powers observed[22]. The high muscle speed and power are consistent with our measurements on contracting skinned fibres from cheetahs[23]. The cheetah deceleration magnitudes (Figs 3d and 4b), cycle works (Fig. 4c) and powers (Fig. 4d) were greater than during acceleration and up to three times higher than polo horses[18]; however, comparative figures are sparse. Cheetah can crouch to engage locomotor muscle to enable these deceleration magnitudes (Fig. 1d), and sliding or colliding with the prey may dissipate some energy.

Grip and manoeuvrability key to hunting success

Hunts involved considerable manoeuvring, with maximum lateral (centripetal) accelerations often exceeding 13 m s^{-2} at speeds less than 17 m s^{-1} (Fig. 4e, f; polo horses achieve 6 m s^{-2}; ref. 3). A lateral acceleration of 13 m s^{-2} (Fig. 1b) requires a coefficient of friction with the ground of at least 1.3. Ridged footpads and substantial claws[24] (Fig. 1c) act as cleats to augment friction and deliver this level of grip. The maximum centripetal acceleration observed was smaller at speeds greater than 17 m s^{-1} (Fig. 4e), which may be behavioural in origin; that is, cheetahs do not perform tight turns at their highest speeds. Studies on other animals show that, although grip limits turning performance at low and moderate speed, a model based on the capacity of the limbs to withstand the combination of centripetal acceleration and gravity (Fig. 1b) is appropriate to account for reduced speed on bends in humans, mice and racehorses[3,25–27] but not greyhounds[2]. The dashed line labelled LFL (leg force limit) in Fig. 4e is calculated using published models[3,25,27], published stride data[7] and the maximum speed recorded here. The equations and assumptions are presented in the Supplementary Information. The LFL line seems to follow the upper bound of the data points at higher speeds, but confident verification would,

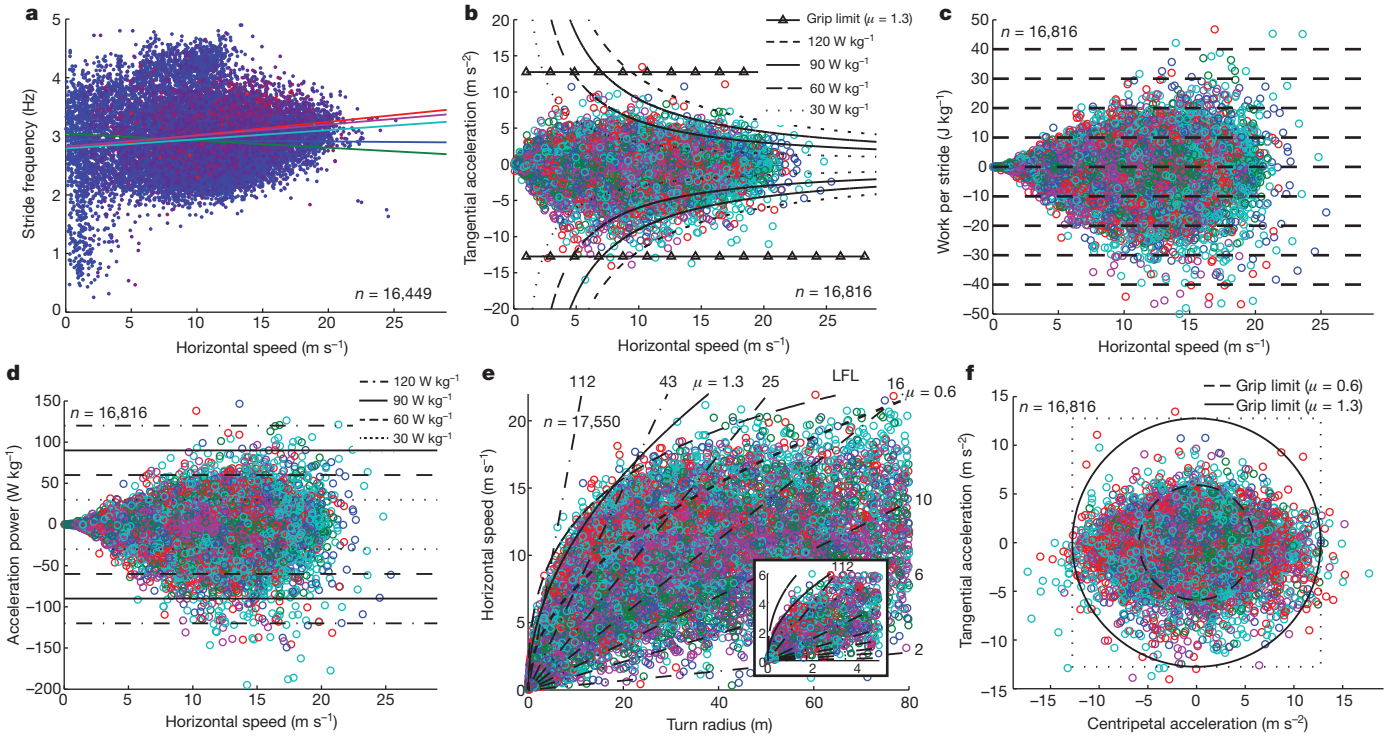

Figure 4 | Performance summary. **a**, Stride frequency plotted against speed; each point is colour-coded for tangential (forwards) acceleration, bright red points represent the greatest forward acceleration, and are plotted last (on top). Lines are linear regression of stride frequency against speed for each individual cheetah. **b**, Tangential (forwards, positive) acceleration and deceleration (*y* axis) against speed (*x* axis). Horizontal lines represent acceleration and deceleration of 13 m s^{-2}, equating to the proposed grip limit of 1.3 (see text). Curved lines represent stride-averaged whole-body powers of ±30, 60, 90 and 120 W kg^{-1}; points outside the outer dashed line equate to a mean stride power in excess of ±120 W kg^{-1}. **c**, Body, mass specific, horizontal kinetic energy change performed in each stride (work per stride). **d**, Stride-averaged whole-body acceleration power plotted against speed, with horizontal lines showing powers of ±30, 60, 90 and 120 W kg^{-1}. **e**, Horizontal speed against turn radius, region around origin magnified in inset. Slanting straight lines show different rates of heading change in degrees per second, with values (2, 6, 10, 16, 25, 43 and 112) at the top of the line. The solid curved line ($\mu = 1.3$) represents a grip limit/coefficient of friction of 1.3; the curved shorter-dashed line ($\mu = 0.6$) denotes the 0.6 grip limit reported for polo horses[3]; points above each line require a higher grip level. The curved longer-dashed line (LFL) represents a limit to turning defined by the maximum force the legs can withstand. **f**, Plot of tangential acceleration against lateral acceleration. Total horizontal acceleration is the distance from the origin, circles represent mean total horizontal acceleration of 6 and 13 m s^{-2} (equating to average grip limits of 0.6 and 1.3). Each point on each plot represents data centred on a single stride, with data smoothed over three strides. Points are colour-coded by individual, except in plot **a**. The number of strides from each cheetah were 5,031, 4,022, 3,211, 2,657 and 1,895 giving a total n of 16,816 for plots **b**, **c**, **d** and **f**. The total *n* is given in each plot and was slightly different for plots **a** and **e** owing to the mathematics of generating those plots but the individual contributions were in proportion.

however, require stance times or limb forces during manoeuvring[26]. When combined with gravity, a lateral acceleration of 13 m s^{-2} equates to a 66% increase in the cheetah's effective weight and hence average limb force (Fig. 1b). Cheetahs have relatively large limb bone cross-sectional areas (compared with greyhounds[20,21]), which may be an adaptation to resist the large peak limb forces that occur during high speed manoeuvring.

The cheetah should run little faster than its prey in the manoeuvring phase of the hunt[28,29] if it is to capture an agile and quick-turning prey. A cheetah running at 25.9 m s^{-1} with the maximal observed lateral acceleration of 13 m s^{-2} would have a turn radius of 52 m and would take 6 s to perform a 180° turn ($\pi r v^{-1}$)—peak running speed is therefore unlikely to be, and was not found to be, a feature of the final stage of successful hunts. A cheetah can slow by 4 m s^{-1} in a stride (Supplementary Fig. 5d), and the cheetahs often decelerated sharply before turning, which would enable much tighter turns. Slowing from 16 m s^{-1} to 4 m s^{-1} (three strides, 1 s) would drop the turn radius with $v^2 r^{-1} = 13$ (lateral acceleration of 13 m s^{-2}) from 19.7 m to 1.2 m, and heading velocity ($v r^{-1}$) would rise from 46 to 190° s^{-1}. This demonstrates the value of slowing down before manoeuvering. The cheetahs did not use highest tangential and centripetal accelerations simultaneously, consistent with grip limiting maximal horizontal acceleration (there are few data points in the corners of the square in Fig. 4f). Rapid deceleration would unload the hindquarters, which could result in yaw instability when manoeuvring because the centre of mass (COM) is behind the forelimbs (like a ground loop in a tail wheel aircraft). The pitch limit proposed in ref. 18 may apply at low speed, but insufficient low-speed data exist to consider this further, and it can be circumvented by posture due to the cheetah's flexible spine (Fig. 1d). The active movements of the high-inertia tail that are observed in wildlife documentaries will help in positioning and banking the body (and limbs) to apply appropriate forces to prevent this and for turn initiation and manoeuvring.

Perspective

Equivalent data for other wild cursorial species would enhance what we know about natural speed, agility, endurance and locomotor physiology, and provide detailed information on ranging behaviour in the wild. For example, such fine-scale data on habitat selection by endangered species detailing where animals are commuting, hunting and resting will be informative when attempting to evaluate landscape scale connectivity, corridors and wildlife-protected areas. Tightly coupled GPS–IMU processing can deliver 0.2-m position accuracy (the level of individual shrubs and footfalls) during hunts, enabling detailed analysis of context variables (such as habitat characteristics and prey visibility), modes of hunting success and failure, and the effect of slope, camber and foot-surface interaction on stride-by-stride performance. These data on hunt environment would inform about

the determinants of preferred hunting habitats, risk of injury (of paramount importance for solitary predators), risk of detection by kleptoparasites (open versus closed habitat), available palatable grazing and habitat-dependent risk of predation (detection).

METHODS SUMMARY

Collars moved between six operating states depending on the time of day, the activity level of the cheetah, and battery voltages (Supplementary Fig. 1). If the cheetah were active (detected via accelerometers) at a time when hunting was likely, accelerometer data samples were continuously buffered in memory, and the GPS module was regularly triggered ('refreshed') to maintain an internal state ready for immediate start-up. When a run started, GPS data at 5 Hz and full IMU data at 300 Hz were recorded. The GPS–IMU data were post-processed in a loosely coupled extended Kalman smoother optimized for sensor characteristics (Methods) and cheetah dynamics. Horizontal position error (median stride-wise standard deviation (s.d.), $n = 45{,}851$) was reduced from 5.05 m (pure GPS data) to 0.67 m in the smoothed solution. Speed error was reduced from 1.23 m s^{-1} to 0.34 m s^{-1} (Supplementary Fig. 3). The initial seconds of the run were reconstructed by open-loop inertial integration, backwards in time, using buffered IMU data and smoothed GPS–IMU data for initial conditions. Data were segmented into strides using the horizontal acceleration signal, and a rolling average was applied to the stride duration, speed and heading rate data (methods) to ensure that cutting did not result in erroneous extreme values in these or derived parameters (Supplementary Fig. 4). Activity summaries, based on accelerometer readings, were recorded for each 30-s period throughout the rest of the day, with a GPS position every 5 min when the cheetah was on the move. The dynamic performance of the collar for track and speed was verified by running a dog on a beach (Supplementary Fig. 2); footprint position in the sand was determined using survey-grade GPS, and footfall time from GPS time-stamped high-speed video.

Full Methods and any associated references are available in the online version of the paper.

Received 15 June 2012; accepted 17 May 2013.

1. Spence, A. J., Thurman, A. S., Maher, M. J. & Wilson, A. M. Speed, pacing strategy and aerodynamic drafting in Thoroughbred horse racing. *Biol. Lett.* **8,** 678–681 (2012).
2. Usherwood, J. R. & Wilson, A. M. Biomechanics: no force limit on greyhound sprint speed. *Nature* **438,** 753–754 (2005).
3. Tan, H. & Wilson, A. M. Grip and force limits to turning performance in competition horses. *Proc. R. Soc. Lond. B* **278,** 2105–2111 (2011).
4. Self, Z. T., Spence, A. J. & Wilson, A. M. Speed and incline during Thoroughbred horse racing: racehorse speed supports a metabolic power constraint to incline running but not to decline running. *J. Appl. Physiol.* **113,** 602–607 (2012).
5. Sharp, N. C. C. Timed running speed of the cheetah (*Acinonyx jubatus*). *J. Zool.* **241,** 493–494 (1997).
6. Hildebrand, M. Further studies on locomotion of the cheetah. *J. Mamm.* **42,** 84–91 (1961).
7. Hudson, P. E., Corr, S. A. & Wilson, A. M. High speed galloping in the cheetah (*Acinonyx jubatus*) and the racing greyhound (*Canis familiaris*): Spatio-temporal and kinetic characteristics. *J. Exp. Biol.* **215,** 2425–2434 (2012).
8. Bissett, C. & Bernard, R. T. F. Habitat selection and feeding ecology of the cheetah (*Acinonyx jubatus*) in thicket vegetation: is the cheetah a savanna specialist? *J. Zool.* **271,** 310–317 (2006).
9. Eaton, R. L. *The Cheetah: The Biology, Ecology, and Behviour of an Endangered Species* Ch.3 (Van Nostrand Reinhold, 1973).
10. Cagnacci, F., Boitani, L., Powell, R. A. & Boyce, M. S. Animal ecology meets GPS-based radiotelemetry: a perfect storm of opportunities and challenges. *Phil. Trans. R. Soc. B.* **365,** 2157–2162 (2010).
11. Tomkiewicz, S. M., Fuller, M. R., Kie, J. G. & Bates, K. K. Global positioning system and associated technologies in animal behaviour and ecological research. *Phil. Trans. R. Soc. B.* **365,** 2163–2176 (2010).
12. Tan, H., Wilson, A. M. & Lowe, J. Measurement of stride parameters using a wearable GPS and inertial measurement unit. *J. Biomech.* **41,** 1398–1406 (2008).
13. Grünewälder, S. *et al.* Movement activity based classification of animal behaviour with an application to data from cheetah (*Acinonyx jubatus*). *PLoS ONE* **7,** e49120 (2012).
14. Caro, T. M. *Cheetahs of the Serengeti Plains* (Univ. Chicago Press, 1994).
15. Mills, M. G. L., Broomhall, L. S. & du Toit, J. T. Cheetah *Acinonyx jubatus* feeding ecology in the Kruger National Park and a comparison across African savanna habitats: is the cheetah only a successful hunter on open grassland plains? *Wildl. Biol.* **10,** 177–186 (2004).
16. Durant, S. M. Competition refuges and coexistence: an example from Serengeti carnivores. *J. Anim. Ecol.* **67,** 370–386 (1998).
17. Broekhuis, F., Cozzi, G., Valeix, M., McNutt, J. W. & Macdonald, D. W. Risk avoidance in sympatric large carnivores: reactive or predictive? *J. Anim. Ecol.* http://dx.doi.org/10.1111/1365-2656.12077 (20 May 2013).
18. Williams, S. B., Tan, H., Usherwood, J. R. & Wilson, A. M. Pitch then power: limitations to acceleration in quadrupeds. *Biol. Lett.* **5,** 610–613 (2009).
19. Cavagna, G. A., Komarek, L. & Mazzoleni, S. The mechanics of sprint running. *J. Physiol.* **217,** 709–721 (1971).
20. Hudson, P. E. *et al.* Functional anatomy of the cheetah (*Acinonyx jubatus*) hindlimb. *J. Anat.* **218,** 363–374 (2011).
21. Hudson, P. E. *et al.* Functional anatomy of the cheetah (*Acinonyx jubatus*) forelimb. *J. Anat.* **218,** 375–385 (2011).
22. Curtin, N. A., Woledge, R. C. & Aerts, P. Muscle directly meets the vast power demands in agile lizards. *Proc. R. Soc. Lond. B* **272,** 581–584 (2005).
23. West, T. G. *et al.* Power output of skinned skeletal muscle fibres from the cheetah (*Acinonyx jubatus*). *J. Exp. Biol.* http://dx.doi.org/10.1242/jeb083667 (11 April 2013).
24. Russell, A. P. & Bryant, H. N. Claw retraction and protraction in the carnivore: the cheetah (*Acinonyx jubatus*) an atypical felid. *J. Zool.* **254,** 67–76 (2001).
25. Usherwood, J. R. & Wilson, A. M. Accounting for elite indoor 200 m sprint results. *Biol. Lett.* **2,** 47–50 (2006).
26. Chang, Y. H. & Kram, R. Limitations to maximum running speed on flat curves. *J. Exp. Biol.* **210,** 971–982 (2007).
27. Greene, P. R. Running on flat turns: experiments, theory, and applications. *J. Biomech. Eng.* **107,** 96–103 (1985).
28. Schaller, G. B. Hunting behaviour of the cheetah in the Serengeti National Park, Tanzania. *Afr. J. Ecol.* **6,** 95–100 (1968).
29. Howland, H. C. Optimal stratagies for predator avoidance: the relative importance of speed and manoeuvrability. *J. Theor. Biol.* **47,** 333–350 (1974).

Supplementary Information is available in the online version of the paper.

Acknowledgements We thank S. Amos and M. Dickson for fabricating collars, and F. Broekhuis, R. Furrer and N. Jordan for working with us in the study area; P. Apps for many discussions; T. Hubel and A. Wills for helping to collect and analyse validation data; P. Apps, J. Usherwood and A. Wilson for comments on the manuscript; and the EPSRC (EP/H013016/1), BBSRC (BB/J018007/1) and DARPA M3 Program (W91CRB-11-C-0048, with Boston Dynamics) for funding. This work was approved by RVC Ethics & Welfare Committee and was carried out under a Botswana Government Research Permit held by J.W.M. and Botswana Veterinary Registration held by A.M.W.

Author Contributions A.M.W. conceived, designed and led the study, A.M.W. and J.C.L. designed the collars, J.C.L. developed collar hardware and software, K.R. developed GPS–IMU filtering, K.R., P.E.H. and A.M.W. analysed data, A.M.W. wrote the paper with input from all authors, K.A.G. and J.W.M. organized field work, monitored animals and downloaded data. A.M.W. performed veterinary work.

Author Information Reprints and permissions information is available at www.nature.com/reprints. The authors declare no competing financial interests. Readers are welcome to comment on the online version of the paper. Correspondence and requests for materials should be addressed to A.M.W. (awilson@rvc.ac.uk).

METHODS

Animals. The cheetahs used in this study were part of a continuing study by Botswana Predator Conservation Trust (http://www.bpctrust.org) in the Okavango Delta region of Northern Botswana. Initially, three 'mark 1' prototype collars were fitted to three cheetahs in July 2011. All collars successfully collected data as intended, two collars for 7–9 months whereas the third suffered a memory card failure after 6 months. Three collars of a new 'mark 2' design were used in April 2012, and two more collars in July 2012 (fitted to the original three cheetahs plus two new individuals). Data were again successfully collected from these collars, and they continue in operation.

The cheetahs were immobilized by free darting from a vehicle by A.M.W. using medetomidine (2 mg) and ketamine (80–120 mg) and reversed after 60 min with 10 mg atipamezole. While sedated, dimensions including limb lengths, thigh girths and back lengths and body mass were recorded. Collar data were downloaded by radio link every few weeks to a ground vehicle or a light aircraft.

Collar design and fabrication. The major design challenges included the measurement and logging of data at a sufficiently high rate and accuracy, timely remote retrieval of substantial volumes of data from the collar and maintaining the very low average power consumption required in a wildlife collar. To conserve power, careful management of the internal readiness of the GPS subsystem allowed this and other sensor systems to be started quickly enough to capture data at maximum rate only during these events.

All collars were constructed in-house. In the original collars (mark 1, used in 2011), a commercial radio-tracking collar (Sirtrack, New Zealand) was used as a base, our custom electronics package being mounted on the top of the collar in a clear cast resin case and wired to the collar's original battery box at the bottom of the collar. The revised mark 2 collars (Fig. 1a) were entirely constructed in-house, with a revised lower-profile electronics enclosure (cast from polyurethane resin using a silicon mould and a rapid prototyped former; Aprocas GmbH) and a vacuum-formed polycarbonate battery box holding larger rechargeable and back-up battery in potting compound. The actual electronics package was similar on both versions, with an identical chip set as described below, and with almost identical software functionality. Collar mass was approximately 340 g.

Collar design: electronics payload. The collar circuit was based around a low-power MSP430 16-bit microcontroller (Texas Instruments), running custom software written in the 'C' programming language developed using an integrated development system from IAR Systems. The microcontroller contains several internal peripheral blocks, including an 8-channel 12-bit analogue-to-digital converter (ADC), four serial communications modules, plus various timers, general-purpose digital input and output lines, and other support modules. A connected 2-GB micro-SD flash memory card (Sandisk) provided data storage.

GPS position was obtained from an LEA-6T GPS module (u-Blox AG). In addition to internally computed position and velocity, the module is able to generate raw pseudo-range, phase and Doppler data for the signal from each satellite enabling detailed GPS performance evaluation, and use of customized differential techniques for increased accuracy. The data rate was five position, velocity and raw data points per second during continuous operation (for example, during a chase).

The collar circuit also included an inertial measurement suite, based on MEMS devices. Acceleration was measured using an MMA7331 three-axis accelerometer module (Freescale Semiconductors), providing acceleration with a $\pm 12\,g$ range. The roll and pitch rotation rate was measured by a dual-axis gyroscope (ST Microelectronics), and yaw rotation rate by a single-axis gyroscope (ST Microelectronics), both set to the $2{,}000^{\circ}\,s^{-1}$ range. Sensor outputs were filtered by simple single-pole analogue filters (100 Hz knee), and then sampled by the microcontroller ADC at 300 or 100 samples per second (Accelerometers or Gyroscopes, respectively). Three-hundred hertz was chosen as giving an overhead to a frequency of 30 Hz; that is, 1/minimum published stance time[7]. A three-axis magnetometer (Honeywell), connected via I^2C, provided magnetic compass functionality at 12 measurements per second.

Primary communication with the collar, for tasks such as data file download and configuration file upload, was via a 2.4-GHz chirp-spread-spectrum communication module (Nanotron Technologies Gmbh), communicating at 1 Mbit per second using a custom communications protocol. A 173-MHz VHF radio transmitter (Radiometrix) provided longer-range transmission of current GPS-derived position, for tracking purposes. An original equipment manufacturer (OEM) conventional wildlife tracking transmitter in the 149-MHz band (Sirtrack) facilitated long-range animal location using conventional direction-finding techniques.

Collar design: power. Primary power supply for the collar was a 900 mAh lithium-polymer rechargeable battery (Active Robots), charged by a solar cell array consisting of 10 monocrystalline silicon solar cells (Ixys Koria). On the mark 2 collars, a 13 Ah lithium thionyl chloride primary battery (Saft) provided a back-up power source (on the original collars, a 7.7 Ah lithium thionyl chloride primary battery was used). Both battery voltages, together with the charge current from the solar cell array, were measured by the microcontroller, which switched the collar electrical load from one battery to the other depending on battery state.

Collar design: software states and movement detection. In operation, the collar software moved between several different operating 'states', the particular state at any moment being dependent on a combination of animal activity level (measured using the accelerometers) and time of day (from a GPS-synchronised software clock). Each state required a different mix of hardware sub-systems to be powered on or off, and different intervals between GPS module operation, and thus the power consumption of the collar varied depending on the operating state. Thus, the inevitable compromise between average power consumption on the one hand, and quantity and resolution of data gathered on the other, could be optimized by setting the parameters for the state transitions. The different operating states and associated average power consumption for the collar are summarized in Supplementary Fig. 1.

To keep the average power consumption as low as possible, the collar would generally default to operating in state 1 ('alert' state). In this state, to detect when the cheetah was moving, the accelerometer was sampled at 30 Hz for a period of 10 s in every minute. Within each 10-s sampling period, the peak-to-peak acceleration was computed for each axis every 2 s, and an accumulator incremented by a specified value for each 2-s window in which the peak-to-peak acceleration exceeded a pre-set threshold; For each 2-s window in which the peak-to-peak acceleration did not exceed the threshold the accumulator was decremented by a (different) specified value. Thus, periods of movement could be given higher 'weight' than periods of no movement or vice versa to identify stalking. If the accumulator total exceeded a specified value, the cheetah was deemed to be consistently moving and the collar switched to a higher operating state, the exact state depending on time of day. A similar algorithm with different weights and thresholds was then used to determine when the animal had settled back to rest, at which time a switch back to the lower state was executed.

When consistently moving between local times of 06:00 and 09:00, and 17:00 and 19:00 (times when hunting was most likely from previous work), the operating state would transition to state 3 ('ready' state). The GPS was refreshed every 30 s and position recorded every 60 s. Accelerometer data were recorded into a circular buffer at 100 Hz, the buffer storing the latest 3 s of data. If the fore–aft accelerometer data then exceeded a threshold equivalent to galloping, state 4 ('chase' state) would be entered. The buffered data were stored and 5 Hz GPS data, 300 Hz accelerometer, 100 Hz gyroscope and 12 Hz magnetometer data recorded. A record was defined as valid if five further peaks (strides) were detected, and then recording would continue until there were no peaks above the threshold for 5 s. When moving consistently but outside of the peak hunting times, the lower-powered state 2 ('mooch' state) would be invoked, with GPS positions being taken every 5 min and simple activity measurements being taken as described below. The GPS delivered a first fix in 1.30 s after triggering (median), accurate position data ($<$10 m s.d.) after 1.58 s, and full rate data (5 Hz) after 5.4 s (Supplementary Fig. 3). The unexpectedly long delay in the GPS module delivering 5 Hz data prevented open-loop GPS–IMU integration back to the beginning of the run in some cases. This is why many runs in Supplementary Video 2 do not start at low speed.

Collar power handling and power consumption. Average collar power consumption varied between individual animals (owing to differing patterns of activity and hence a different distribution of collar operating states), but was typically around 4 mA when averaged over 24 h. The main contributor to this average was the time spent in the ready state when the animal was active during hunting times of day (Supplementary Fig. 1), in which average consumption was around 16 mA with a 30-s GPS refresh time. By comparison, the time spent in the mooch state (animal active but outside hunting times) had a lower consumption of about 5 mA, whereas 'sleep' or alert states (animal inactive) contributed only about 0.6 mA. The 'chase' state, used only when the animal is running, required some 90 mA, but time spent in this state was very small. Solar charge currents ranged from 35 mA with the animal in full sunlight, to typically 10 mA in dappled shade and almost zero in deeper shade. Average charge current over a 24-h period was typically 2 mA, with some variation between animals due to terrain preferences, indicating little time spent in full sunlight even in the winter study period. The solar cells, via the rechargeable battery, contributed roughly 75% of the collar power, the remainder being supplied by the non-rechargeable battery. Collar battery life was predicted at approximately one year with these settings, but was very dependent on collar settings and animal behaviour.

On cheetahs four and five, the ready state GPS refresh interval was changed from 30 s to 300 s—this resulted in a typical power saving of around 30% over a 24-h period, with unexpectedly little effect on GPS start-up time (Supplementary Fig. 3f). We reduced power consumption on mark 2 collars (254 runs) by not

pre-buffering data, and moving directly from mooch to chase state (and allowing this to happen at any time of day, enabling Fig. 3e to be generated), so that IMU data logging began on the first accelerating stride when the cheetah was already in motion. The time that could be recovered through backwards integration was therefore reduced, and the first 1–2 acceleration strides lost.

Collar design: generation of activity summaries. Throughout all states, a background measurement of animal activity was also recorded. For every 2-s 'window', the maximum peak-to-peak acceleration range is recorded separately for all three accelerometer axes. After 15 'windows' have passed, an activity record is generated, containing GPS time, the largest *X*, *Y* and *Z* peak-to-peak acceleration amplitudes seen in any of the 15 windows, and the average of the 15 2-s peak-to-peak *X*, *Y* and *Z* accelerations amplitudes. This enabled differentiation of transient high acceleration events and consistent activity. This record is generated continuously in the mooch and ready state, every 3 min in the alert state, and every 30 min in the sleep state. Amplitudes are higher than body acceleration, because the collar can move relative to the centre of mass.

All settings that affected the state transitions (times, acceleration thresholds, and so on), and many other settings besides, could be modified by uploading a new configuration file over the 2.4-GHz communications link. In addition, a complete new version of the collar firmware could be uploaded over this link, allowing for in-field program updates while the collar is on the animal.

Sensor fusion and signal processing to capture hunting dynamics. In the collar data collected here, the power management features used gave different sampling rates for accelerometer (300 Hz) and gyro (100 Hz) in the chase state. To capture the full acceleration profile within the microcontroller, 3 s of accelerometer measurements were continually buffered in ready state at a reduced sampling frequency (100 Hz) and recorded when entering the chase state (gyro-power consumption was too high to permit continuous pre-buffering). GPS position and velocity measurements were usually (but not always) available within 1 s after entering the chase state (Supplementary Fig. 3).

The unique characteristics of these data required a custom-designed GPS–INS (inertial navigation system) integration method written in Visual C++ and MATLAB. Calibrated IMU measurements were first linearly interpolated to 300 Hz. Orientation changes were assumed to be minimal during the buffer period, and hence the unmeasured gyro angular rates assumed to be zero. GPS and IMU measurements were fused using a 12-state extended Kalman filter[30] in loosely coupled architecture. The total state formulation used propagates position, velocity and orientation states with time using the IMU measurements in a simplified form of the strap-down inertial navigation equations[31]. The associated process noise was estimated from the known error characteristics of the inertial sensors used. GPS position and velocity updates were used as measurement updates, and receiver accuracy data for each fix used to estimate measurement noise to appropriately weight the GPS to the inertial solution.

The filter was run in reverse time from the last GPS observation of each run to the beginning of the buffered inertial data. During the short time period in which only inertial data was present (throughout buffer and between GPS measurements), the filter propagation was equivalent to open-loop inertial navigation. The filter was initialised using last GPS position and velocity data, and Euler angles assumed zero with covariances appropriate for the uncertainty in that assumption. A Rauch-Tung-Striebel (RTS) smoother[32] was then applied in forward time on the Kalman-filtered data. This is equivalent to combining backward and forward solutions, effectively halving the open-loop INS integration period between GPS observations. It was not always possible to reconstruct the period before the first GPS observation, as this period was often too long or the accuracy of the initial GPS observations insufficient (Supplementary Fig. 3c–f). This will result in a somewhat short measurement of hunt distance in those cases (apparent qualitatively in Supplementary Video 2).

GPS–INS processing was used to reduce noise and improve precision in the position and velocity solution (Supplementary Fig. 3), as well as increasing the temporal resolution of the data. It also allowed determination of orientation, which is otherwise not directly measured. Because the GPS receiver also records raw pseudorange, Doppler and carrier phase measurements for each satellite, future data processing may use a stationary reference station to calculate a more accurate differential GPS solution. Use of a tightly coupled GPS–INS solution may also provide increased accuracy and robustness, especially during periods when a reduced number of satellites are tracked (for example, turns).

Extraction of parameters for analysis: speed, distance and stride timing. Stride timings for data cutting and stride frequency were determined from the axis of accelerometer aligned approximately in the cranio-caudal direction. These accelerations were first low-pass filtered at twice anticipated stride frequency (8 Hz), and a peak detection algorithm was used to detect forward acceleration peaks at minimum duration of 0.2-s apart (equal to a maximum stride frequency of 5 Hz).

Horizontal speed was calculated from filtered velocity and averaged over the calculated strides (v_i) to remove the effects of speed fluctuation through the stride and collar oscillation relative to the centre of mass. These data were then smoothed with a rolling average (see below). Run distance was calculated by zero-order hold integration of the stride averaged horizontal speeds over the duration of the run. Maximum speed during each run was determined from these values. Stride frequency was calculated from the duration between stride timing peaks. For consistency in comparison, other parameters were then determined using the same method as in ref. 3, using only two-dimensional position and speed measurements. Position data were first down-sampled to the calculated stride times. The displacement vectors between consecutive positions were then calculated:

$$\overrightarrow{P_{i-1}P_i} = \overrightarrow{P_i} - \overrightarrow{P_{i-1}}$$

and

$$\overrightarrow{P_iP_{i+1}} = \overrightarrow{P_{i+1}} - \overrightarrow{P_i}$$

in which $\overrightarrow{P_i}$ is the two-dimensional position at sample/stride i.

Extraction of parameters for analysis: acceleration and power. A signed change of heading ($\Delta\theta_i$), and hence heading angular velocity (ω_i), were then calculated from the angle between the two vectors:

$$\Delta\theta_i = \sin^{-1}\left(\frac{\left|\overrightarrow{P_iP_{i+1}} \times \overrightarrow{P_{i-1}P_i}\right|}{\left|\overrightarrow{P_iP_{i+1}}\right|\left|\overrightarrow{P_{i-1}P_i}\right|}\right)$$

and

$$\omega_i = \frac{\Delta\theta_i}{\Delta T}$$

in which ΔT is the sampling interval.

The tangential or forward acceleration ($a_{t,i}$) and centripetal acceleration ($a_{c,i}$), as well as instantaneous turn radius (r_i) were then calculated:

$$a_{t,i} = \frac{v_{i+1} - v_i}{\Delta T}$$

$$a_{c,i} = \frac{v_i^2}{r_i} = \omega_i v_i$$

$$r_i = \frac{v_i}{\omega_i}$$

Finally mass-specific COM power was calculated as the dot product of stride averaged acceleration and stride averaged velocity (that is, multiply forward acceleration by forward speed):

$$k_i = a_i v_i$$

Mass-specific COM stride work (net COM kinetic energy change in a stride) was calculated as change in speed over a stride multiplied by stride average speed.

Extraction of parameters for analysis: improving accuracy through averaging. One important consideration when calculating heading, change of heading, and heading angular velocity from position measurements is that accuracy will decrease as speed decreases. Although averaging over a stride and across strides markedly improves the accuracy, lower average speed values will still be less accurate. The noise present is of a level that does not unduly influence extreme values even at very low speeds.

Although validations carried out on the stride timing show that it is generally accurate (Supplementary Fig. 2f), detection of an incorrect or spurious peak for end of stride would result in one stride duration being under or overestimated, and the adjacent stride duration being affected in the opposite manner. This would introduce error in parameters that do not change smoothly through a stride, such as acceleration and kinetic energy. We therefore applied a weighted average in which the stride period was averaged, with the mean of the duration of the preceeding and following stride. The weighted average was of the form:

$$S_{i,w} = 0.5S_{i-1} + S_i + 0.5S_{i+1}$$

in which S represents the parameter being weighted, and i is the stride number.

This approach was used as follows: tangential acceleration and hence acceleration power were calculated based on a weighted average stride speed. Centripetal acceleration was based on weighted stride speed and weighted heading rate. Stride duration was also weighted. Where these parameters have been plotted against horizontal speed, the weighted stride speed was also used. Applying more averaging than this did not change the distribution of outliers to a discernible extent

(Supplementary Fig. 4), but applying no averaging did result in more outliers giving us confidence in our extreme values with this treatment.

Extraction of parameters for analysis: grip and manoeuvring. Maximum traction has been proposed as a potential constraint to turning performance[3]. Coefficient of friction, μ, is the maximum achievable ratio of horizontal force (acceleration) with respect to vertical force (acceleration). Average vertical force is equal to acceleration due to gravity and assuming that vertical and horizontal forces are always in proportion:

$$\mu \geq \frac{ma}{mg}$$

So that maximum horizontal force and horizontal acceleration (a) are:

$$ma_{\max} = \mu mg$$

$$a_{\max} = \mu g$$

in which g is acceleration due to gravity, and m is mass. Substituting for horizontal acceleration in terms of tangential (a_t) and centripetal components (a_c):

$$\sqrt{a_t^2 + a_c^2} = \mu g$$

This demonstrates the potential trade-off between tangential and centripetal accelerations. Given that maximum centripetal acceleration will occur at constant speed ($a_t = 0$), and likewise that maximum tangential acceleration will occur in a straight line ($a_c = 0$):

$$a_{c,\max} = \mu g$$

$$a_{t,\max} = \mu g$$

Remembering that centripetal acceleration:

$$a_c = \frac{v^2}{r}$$

in which v is horizontal speed, and r is radius of turn. We form an equation for maximum speed ($v_{\max}$) in terms of turn radius (r):

$$\frac{v_{\max}^2}{r} = \mu g$$

$$v_{\max} = \sqrt{\mu g r}$$

A maximum limit for tangential acceleration based on maximum available muscle power (K) is derived as follows. When force and velocity are in the same direction:

$$K = Fv$$

$$K = ma_t v$$

Where F is force magnitude, v is horizontal speed, a_t is tangential acceleration and m is body mass. Given specific power by body mass (k):

$$k = \frac{K}{m}$$

Substituting gives:

$$a_{t,\max} = \frac{k_{\max}}{v}$$

Geometric limit to acceleration. A pitch limit for acceleration was previously proposed[20] that assumes that propulsion is derived purely from hip extension. This gives an acceleration limit for greyhounds of 10 m s^{-2} at all speeds derived from back length and leg length, and the limit for cheetahs would be similar as body height and length are similar[7]. Such a limit is not exceeded in our data (Fig. 4b), but there are few low speed acceleration strides.

Collar validation. A lurcher (greyhound/whippet/terrier cross in this case) dog was fitted with a mark 2 collar and encouraged to undertake maximal accelerations and sharp running turns on a beach in England, UK (the dog was accustomed to collar-testing experiments). The position of each footfall was determined using Survey grade GPS (OEM4, Novatel). Dual frequency Doppler and pseudorange and phase GPS data were post-processed relative to a local base station data using Waypoint GrafNav 8.10 (Novatel) with a horizontal accuracy of 20 mm. The timing of each footfall was determined from simultaneous high-speed video at 500 frames per second (f.p.s.) (X-Pri 1280 × 1024 AOS Gmbh). The camera trigger event was captured via an interrupt channel on an RVC GPS logger module with sub-millisecond accuracy, and used to express footfall events in GPS time for comparison to collar data (Supplementary Fig. 2e). The four footfalls per stride were easily identified in the position data (Supplementary Fig. 2a, b), and the distance between subsequent non-lead forefootfalls was defined as stride length, and the time between those foot falls as stride duration. Stride duration by video and by processing of collar data was compared by subtracting stride time from foot falls on high-speed video from stride duration from collar data and plotting the difference as a histogram (Supplementary Fig. 2f). Speed was calculated by dividing stride length by stride duration, and data were smoothed with a three-stride centre weighted rolling average as described for the collar data and the results plotted (Supplementary Fig. 2d). These data show that qualitatively the collar reproduces the track of the footfalls and that the speed time (and hence acceleration) data are indistinguishable between the two approaches. Further trials and analysis are required for a full assessment of the two methods.

Statistics. To establish which aspects of a run correlate with success, GLMMs were performed in R statistical software (R, version 2.14.1, 2011. R Development Core Team 2011, Foundation for Statistical Computing, Vienna, Austria). In the model, all the descriptive parameters of each hunt (terrain, distance, top speed, peak acceleration and deceleration number of turns and total turn angle) were included as fixed effects. To control for individual variation, a subject was included as a random effect. If an effect was not significant, and removing it from the model improved the Akaike information criterion (AIC), then it was removed. A chi-squared test was used to evaluate the effect of terrain on outcome.

Human acceleration power. Ten-metre split times for the 9.58 s world 100-m record run by Usain Bolt in 2009 were retrieved from the IAAF website (http://berlin.iaaf.org/records/biomechanics/index.html). A fifth order polynomial was fitted through the distance–time data. This polynomial visually fitted the data points and was differentiated to give formulae for speed and acceleration through the race and a function for instantaneous power through the race calculated as the product of the functions for speed and acceleration. This gave a peak centre of mass power of 25 W kg^{-1} body mass at 7 m s^{-1}, which is similar to previously published values for human sprinters[19].

Hunting, terrain and outcome (success). Runs were identified in activity summaries by very high-peak acceleration amplitudes in all three axes, but particularly high accelerations in the cranio-caudal direction were the best indicator, confirmed from GPS speed where present. If two run events were within 10 min of one another, they were considered to be the same event for outcome measures. Terrain was determined from Google Earth; georeferencing of known landmarks and road junctions was confirmed to be accurate to within 5 m in the study area.

We identified feeding as a consistent signal on all three accelerometer axes (mean amplitude similar to mean of mean amplitudes), with particularly low cranio-caudal accelerations (compared with walking) and no change in location. See ref. 13 for more discussion. We classified a run as a successful hunt if 6 min of this feeding behaviour occurred in the 30 min after a run was identified. These methods correctly identified nine out of the ten known successful hunts using only the activity data (that is, without using GPS data), and correctly identified all nine as successful hunts. When applied to the main data set, the classification outcome correlated to other markers of success in 97% of known hunts. The other markers were: prey struggling captured in the accelerometer signal; cheetah remaining at hunt location for over two hours after the run; observing the cheetah on a kill.

List of symbols. i, stride number; $\overrightarrow{P_i}$, two-dimensional position; $\Delta\theta_i$, signed change of heading; ω_i, heading angular velocity; ΔT, sampling interval; a_i, horizontal acceleration; $a_{t,i}$, tangential or forward acceleration; $a_{c,i}$, centripetal acceleration; r_i, instantaneous turn radius; v_i, stride averaged horizontal speed; K, whole-body power; k_i, mass-specific whole-body power; S_i, parameter to be weighted; $S_{i,w}$, parameter after weighting; μ, coefficient of friction; m, body mass; g, acceleration due to gravity.

30. Kalman, R. E. A new approach to linear filtering and prediction problem. *Trans. ASME J. Basic Engineering* **82D,** 34–45 (1960).
31. Titterton, D. H. & Weston, J. L. *Strapdown Inertial Navigation Technology* 2nd edn, Vol. 207, Chs 3 and 11 (AIAA, 2004).
32. Rauch, H. E., Tung, F. & Striebel, C. T. Maximum likelihood estimates of linear dynamic systems. *AIAA J.* **3,** 1445–1450 (1965).